iScience

CellPress
OPEN ACCESS

Article

Activation of cGAS/STING pathway upon paramyxovirus infection

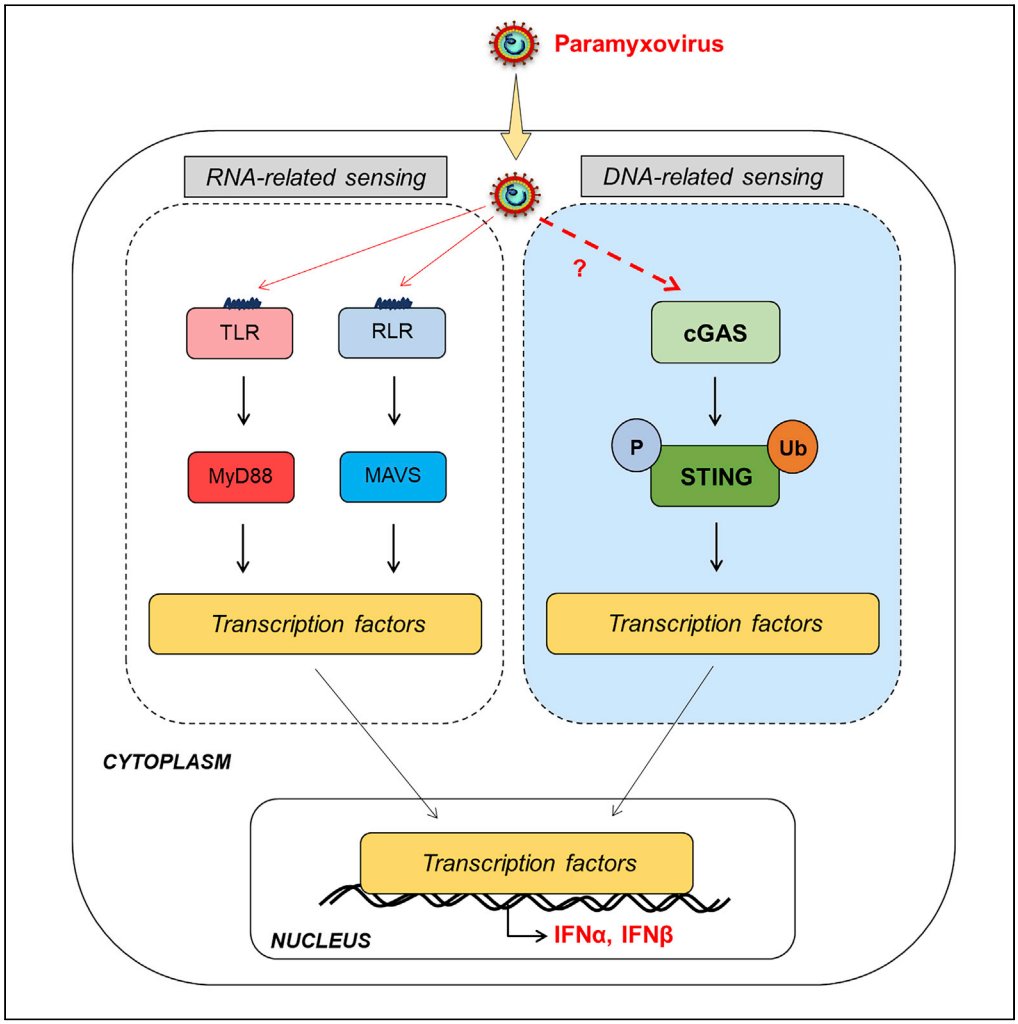

Mathieu Iampietro, Claire Dumont, Cyrille Mathieu, ..., Denis Gerlier, Ulrich Kalinke, Branka Horvat

mathieu.iampietro@inserm.fr (M.I.)
branka.horvat@inserm.fr (B.H.)

Highlights

RNA sensors are insufficient for the effective control of paramyxovirus infection

STING adaptor protein is involved in controlling Nipah virus infection in mice

cGAS/STING axis is primordial for optimal production of IFN-I against NiV and MeV

STING protein can be activated during infections by RNA viruses

Iampietro et al., iScience 24, 102519
June 25, 2021
https://doi.org/10.1016/j.isci.2021.102519

iScience

CellPress
OPEN ACCESS

Article

Activation of cGAS/STING pathway upon paramyxovirus infection

Mathieu Iampietro,[1,5,*] Claire Dumont,[1] Cyrille Mathieu,[1] Julia Spanier,[2] Jonathan Robert,[1] Aude Charpenay,[1] Sébastien Dupichaud,[1] Kévin P. Dhondt,[1] Noémie Aurine,[1] Rodolphe Pelissier,[1] Marion Ferren,[1] Stéphane Mély,[3] Denis Gerlier,[1] Ulrich Kalinke,[2,4] and Branka Horvat[1,*]

SUMMARY

During inflammatory diseases, cancer, and infection, the cGAS/STING pathway is known to recognize foreign or self-DNA in the cytosol and activate an innate immune response. Here, we report that negative-strand RNA paramyxoviruses, Nipah virus (NiV), and measles virus (MeV), can also trigger the cGAS/STING axis. Although mice deficient for MyD88, TRIF, and MAVS still moderately control NiV infection when compared with wild-type mice, additional STING deficiency resulted in 100% lethality, suggesting synergistic roles of these pathways in host protection. Moreover, deletion of cGAS or STING resulted in decreased type I interferon production with enhanced paramyxoviral infection in both human and murine cells. Finally, the phosphorylation and ubiquitination of STING, observed during viral infections, confirmed the activation of cGAS/STING pathway by NiV and MeV. Our data suggest that cGAS/STING activation is critical in controlling paramyxovirus infection and possibly represents attractive targets to develop countermeasures against severe disease induced by these pathogens.

INTRODUCTION

The innate immunity represents the first line of host defense against invading pathogens (Akira et al., 2006). Exogenous motifs associated with viral infections involved in stimulating innate responses include pathogen-derived nucleic acids, DNA, or RNA (Akira et al., 2006; Mogensen, 2009). Its ensuing detection activates pattern recognition receptor (PRR)-associated adaptor molecules that are responsible for subsequent expression of type I and III interferons (IFNs) (Park and Iwasaki, 2020) and the induction of IFN-related genes, which are important for the control of virus infection (Borden et al., 2007; Der et al., 1998; Sen and Peters, 2007). Four major axes, defined by their nodal adaptor, are able to induce strong innate immune responses upon sensing of pathogen-related nucleic acids (Baccala et al., 2009). Three of them, Toll-like receptor (TLR)-associated adaptor molecules: myeloid differentiation primary response 88 (MyD88) (Wesche et al., 1997), Toll/interleukin-1 receptor/resistance [TIR] domain-containing adaptor-inducing IFN-β (TRIF) (Yamamoto et al., 2003), and RIG-I-like receptor (RLR)-associated mitochondrial antiviral signaling protein (MAVS), (Seth et al., 2005) are dedicated to sense DNA and/or RNA. The cyclic guanosine monophosphate-adenosine monophosphate (cGAMP) synthase (cGAS)/stimulator of interferon genes (STING also known as ERIS, MITA, or TMEM173) pathway is the leading sensor for the detection of cytosolic DNA (Ishikawa and Barber, 2008; Sun et al., 2013). The cGAS/STING axis seems to be involved in the sensing of various different RNA viruses, which may express viral proteins that counteract cGAS/STING activity at different levels. Thus the cGAS/STING pathway may also contribute to the control of RNA viruses (Ni et al., 2018). Recently, activation of the cGAS/STING pathway has been observed following infection by the positive-strand RNA virus severe acute respiratory syndrome coronavirus 2 (SARS-CoV-2) (Neufeldt et al., 2020).

In recent years, members of the Paramyxoviridae family have caused numerous emerging zoonoses and/or epidemics (Thibault et al., 2017). This viral family contains both old and new human and zoonotic viral pathogens such as measles virus (MeV) and Nipah virus (NiV). Although MeV has been almost eradicated from most developed countries through vaccination campaigns, the number of cases and deaths significantly increased within the last decade killing more than 100.000 people every year (Ferren et al., 2019). Moreover, as NiV is the most virulent paramyxovirus with mortality rates between 40% and 100% during epidemics and

[1]CIRI, Centre International de Recherche en Infectiologie, INSERM U1111, CNRS, UMR5308, Univ Lyon, Université Claude Bernard Lyon 1, École Normale Supérieure de Lyon, 21 Avenue Tony Garnier, 69007 Lyon, France

[2]Institute for Experimental Infection Research, TWINCORE, Centre for Experimental and Clinical Infection research, a joint venture between the Hanover Medical School and the Helmholtz Centre for Infection Research, Hanover, Germany

[3]INSERM- Laboratoire P4 Jean Mérieux-21 Avenue Tony Garnier, 69365 Lyon, France

[4]Cluster of Excellence-Resolving Infection Susceptibility (RESIST), Hanover, Germany

[5]Lead contact

*Correspondence: mathieu.iampietro@inserm.fr (M.I.), branka.horvat@inserm.fr (B.H.)

https://doi.org/10.1016/j.isci.2021.102519

remains without any licensed treatment or vaccine (Pelissier et al., 2019; Soman Pillai et al., 2020), the World Health Organization included it in its blueprint for priority pathogens (Mehand et al., 2018).

Our previous work evaluating innate sensors involved in the protection of mice following NiV infection suggests control of the virus through the activation of MyD88 and MAVS pathways, whereas TRIF seems dispensable (Iampietro et al., 2020). Although, both MyD88 and MAVS are important to produce high levels of type-I IFNs (IFN-I), double knockout (KO) mice still exhibit some resistance against NiV infection. This is in contrast to the interferon-α/β receptor (IFNAR) KO mice that lack any IFN-I-related responses and are unable to control NiV infection (Dhondt et al., 2013; Iampietro et al., 2020). We thus hypothesized that the cGAS/STING axis of the innate immunity could also contribute to the control of NiV infection.

Once activated in the cytoplasm of infected cells, cGAS uses adenosine triphosphate (ATP) and guanosine triphosphate (GTP) as substrates for cyclization into cGAMP. cGAMP triggers STING and further results in IFN-I expression (Ishikawa and Barber, 2008; Sun et al., 2013). Successive conformational changes ensure the activation of cGAS and STING in cascade. Briefly, cGAS in "resting" state is a monomer containing a conserved zinc-ion-binding domain as DNA-binding module (Civril et al., 2013; Kranzusch et al., 2014). Upon DNA binding in the cytoplasm, cGAS dimerizes and further oligomerizes to induce optimal cGAMP production (Gao et al., 2013; Zhang et al., 2014). Thereafter, cGAMP binds to STING in its ligand-binding domain and induces inward rotations leading to dimerization and later oligomerization of STING (Cong et al., 2019; Ergun et al., 2019; Shang et al., 2012). In addition, upon binding of cGAMP, STING exits the endoplasmic reticulum to the Golgi apparatus. There, it transduces a downstream signaling pathway by recruiting TANK-binding kinase 1 (TBK1) and IRF-3 (but not IRF-7) transactivator and activating the nuclear factor (NF)-κB pathway that results in the activation of type I IFN and cytokine genes (Dobbs et al., 2015; Gui et al., 2019; Liu et al., 2015). The recruitment of IRF-3 relies on the phosphorylation of STING on its Ser366 (Ser365 in murine) by TBK1 (Tsuchiya et al., 2016). In addition, the E3 ubiquitin ligases TRIM32 and TRIM56 promote the non-degradative K-63-linked ubiquitination of Lys224 of STING to trigger a cytokine response (Ni et al., 2017; Tanaka and Chen, 2012). As a third type of post-translational modifications (PTMs) STING palmitoylation governs its trafficking to the Golgi (Mukai et al., 2016).

We report here that both cGAS and STING are required for mounting an efficient innate immune response upon NiV and MeV infection. In infected cells, STING is phosphorylated on S366 (S365 in mouse) and is K63 linked ubiquitinated, confirming the presence of its activated form at later time points following RNA virus infection, similarly to what has been observed by others after infection with DNA virus (Chiang and Gack, 2017).

RESULTS

STING plays a role in the control of NiV infection in mice

Our previous study revealed a complementary role of MyD88 and MAVS in the partial containment of NiV, suggesting that the complete resistance of mice against NiV involves an additional activation pathway of the IFN-I response (Iampietro et al., 2020). The cGAS/STING axis has recently emerged as critical in the cross-talk between innate sensing of cytosolic DNA and RNA viruses (Ni et al., 2018). We therefore analyzed the susceptibility of mice bearing gene deletions in both single TLR and IL-1R (MyD88 KO) pathway, or in combination with TRIF (MyD88/TRIF KO), MAVS (MyD88/TRIF/MAVS KO), and STING (MyD88/TRIF/MAVS/STING KO) signaling platforms (Figures 1 and S1). The animals were infected intraperitoneally and monitored during 24 days for clinical signs and/or death. Infected wild-type (WT), MyD88 KO, and MyD88/TRIF KO mice did not manifest any clinical sign of disease, whereas triple MyD88/TRIF/MAVS KO and quadruple MyD88/TRIF/MAVS/STING KO mice exhibited symptoms of neurological disorders similar to those observed in IFNAR KO mice (Figure 1A). Moreover, whereas 60% triple KO mice survived NiV challenge, all mice bearing the quadruple deficiency succumbed by day 11 post-infection, indicating a crucial and non-redundant role for STING in the protection of mice (Figure 1A). NiV nucleoprotein (NiV-N) protein levels in the brain of autopsied animals deficient for MyD88/TRIF/MAVS and MyD88/TRIF/MAVS/STING were comparable to those observed in the brain of IFNAR KO mice at the time of death (Figure 1B). Furthermore, whereas analysis of NiV load in murine brain determined equivalent NiV-N RNA levels within these three deficient murine models (Figure 1C), evaluation in the spleen showed higher viral loads in mice bearing the quadruple deficiency compared with the triple KO mice (Figure S1A). In parallel, the lower production of IFNβ (Figures 1D and S1B) and less efficient expression of IFNα (Figures 1E and S1C) in the brains and spleens of MyD88/TRIF/MAVS KO and MyD88/TRIF/MAVS/STING KO mice compared with WT were

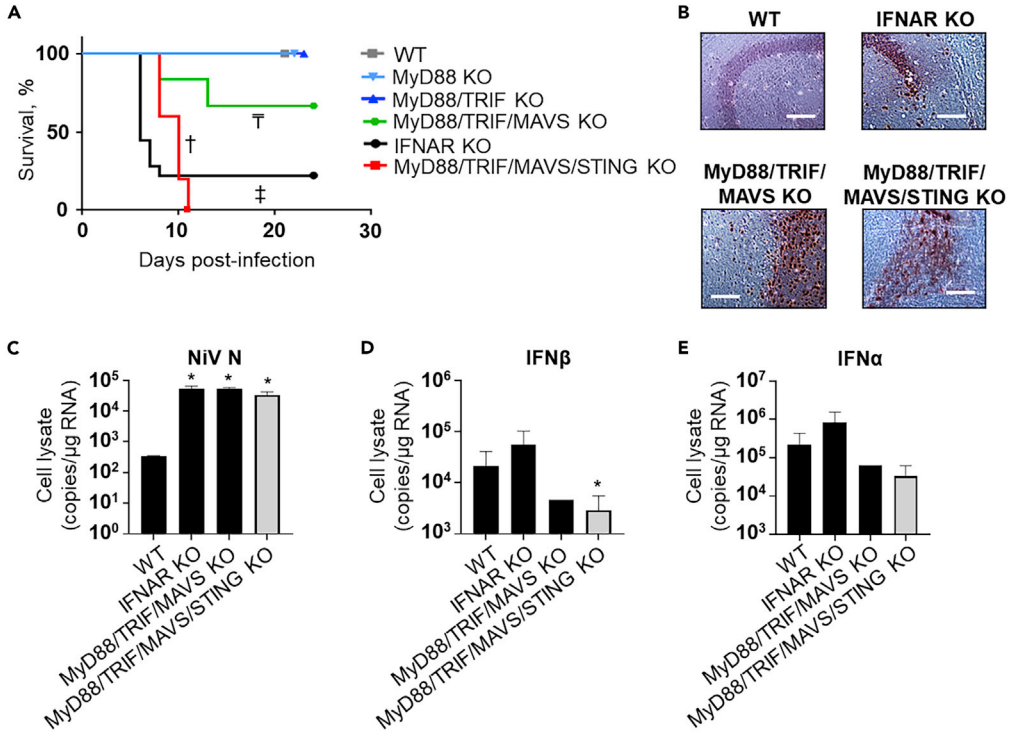

Figure 1. STING plays a role in the control of NiV infection in mice

Wild-type (WT) mice and mice deficient in indicated pathogen recognition signaling pathways were infected intraperitoneally with 10^6 plaque-forming unit (PFU) of NiV (5 or 6 animals per group).

(A) Survival of mice infected by NiV was followed up for 24 days. †$p < 0.05$ (MyD88/TRIF/MAVS/STING KO versus WT), ‡$p < 0.05$ (IFNAR KO versus WT), and $p < 0.01$ (MyD88/TRIF/MAVS KO versus MyD88/TRIF/MAVS/STING KO) (Gehan-Breslow-Wilcoxon test).

(B) Immunohistochemistry of murine brains following NiV infection. Brains of WT mouse, IFNAR KO mouse, MyD88/TRIF/MAVS KO, and MyD88/TRIF/MAVS/STING KO were collected on days 2, 6, 13, and 11, respectively. Scale bars, 100 µm.

(C–E) Expression of NiV nucleoprotein (NiV-N) in the brain of NiV-infected mice, harvested on the day of death or euthanized at the end of protocol for different genotypes, was determined by RT-qPCR. Data are represented as mean ± SEM. Analysis of IFNβ and IFNα expression by RT-qPCR in organs harvested 2–13 days after infection. All samples were analyzed using one-way analysis of variance, followed by the Tukey multiple comparisons test, *$p < 0.05$ compared with WT condition.

associated with their inability to clear the virus. Overall, these results confirm our previous observations on the importance of the RLR signaling platform involving MAVS (Iampietro et al., 2020) and suggest a novel synergistic and non-redundant role of the STING pathway during NiV infection.

STING controls NiV replication in primary murine embryonic fibroblasts

To further evaluate the role of STING during NiV infection in mice, we analyzed the impact of the gene deletion of various nodal adaptors on the *in vitro* NiV replication in primary murine embryonic fibroblasts (pMEFs). The pMEFs were generated from mice bearing the corresponding deleted genes as described previously (Brune et al., 2001). They were infected with rNiV-eGFP to allow imaging of viral infection by fluorescent microscopy. In agreement with above *in vivo* observations, MyD88 KO and MyD88/TRIF KO pMEFs were able to control NiV replication as well as WT pMEFs, with only few observed infected cells. In contrast, NiV rapidly spread within the culture of MyD88/TRIF/MAVS KO and MyD88/TRIF/MAVS/STING KO pMEFs, although not as extensively as in IFNAR KO cells (Figure 2A). Moreover, single STING KO pMEFs were unable to control viral spread, highlighting a major role of STING into mouse innate defense against NiV infection (Figure 2A). The poor permissiveness of WT, MyD88 KO, and MyD88/TRIF KO cells was confirmed by a low amount of viral RNA in these cells (Figure 2B) and limited release of viral RNA in the supernatant (Figure 2C). These three cell types exhibited comparable amounts of IFNβ mRNA (Figure 2D), whereas this mRNA was nearly undetectable in non-infected WT cells. However, contrary to WT pMEFs, which exhibit a

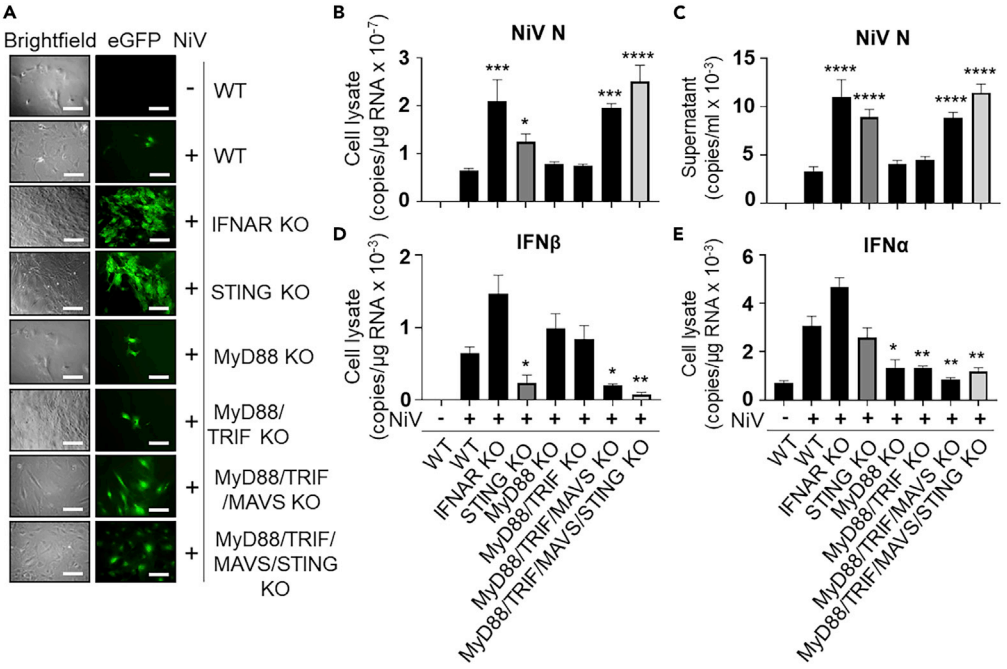

Figure 2. STING controls NiV replication in primary murine embryonic fibroblasts (pMEFs)

pMEFs obtained from mice deficient in the indicated signaling pathways were infected with rNiV-eGFP (MOI of 0.3) and cultured for 24 h.

(A) Cells were analyzed for eGFP expression by fluorescence microscopy. Scale bars, 100 µm.

(B–E) Cells and supernatants were harvested and analyzed by RT-qPCR for NiV-N (B and C), IFNβ (D), and IFNα (E) expression. Data are represented as mean ± SEM. The statistical significance of differences between infected wild-type (WT) cells and knockout (KO) cells was analyzed using one-way analysis of variance, followed by the Tukey multiple comparisons test. *p < 0.05; **p < 0.01; ***p < 0.001; ****p < 0.0001 compared with NiV-infected WT condition.

significant increase in IFNα, the infection of MyD88 KO and MyD88/TRIF KO cells did not result in a significant accumulation of IFNα mRNA (Figure 2E). The infection of IFNAR KO cells was associated with both elevated cytoplasmic and released viral RNA. Moreover, elevated levels of both IFNβ and IFNα mRNA were detected because all four induction axes of innate immunity are functional but unable to activate an efficient antiviral program (Figures 2B–2E). In contrast, no accumulation of either IFNβ or IFNα occurred concurrently to the high levels of NiV-N RNA (Figures 2B and 2C) observed in both infected MyD88/TRIF/MAVS KO and MyD88/TRIF/MAVS/STING KO (Figures 2D and 2E). In STING KO pMEFs, despite lower levels compared with IFNAR KO cells, high amounts of NiV-N RNA accumulated in the cytoplasm compared with WT cells (Figure 2B). This intermediate phenotype of STING KO cells was associated with no significant IFNβ mRNA induction, but high levels of IFNα mRNA (Figures 2D and 2E). Altogether, these results indicate that in murine pMEFs (1) the control of NiV infection is mediated mainly by the IFNβ rather than the IFNα response; (2) STING is necessary for the induction of IFNβ, but not IFNα; and (3) MAVS, in combination with MyD88 or not, is important for the activation of IFN-I genes confirming our previous observations (Iampietro et al., 2020).

cGAS/STING pathway has a critical role in the control of paramyxovirus infection in human THP-1 cells

The role of STING and its upstream activator cGAS in the innate response to NiV was further explored in the human monocytic THP-1 cell line that was either WT or deficient in cGAS (cGAS KO) or STING (STING KO). WT THP-1 cells have the advantage of exhibiting a limited permissiveness to infections with both NiV and the WT-derived recombinant MeV strain rMeV-EdmH-eGFP, another member of the Paramyxoviridae family belonging to the closely related *Morbillivirus* genus. This virus expresses the Edmonston vaccine-derived H glycoprotein allowing the use of ubiquitously expressed CD46 as cellular receptor (Naniche et al., 1993) and hence entry into THP-1 cells that do not or minimally express the known physiological

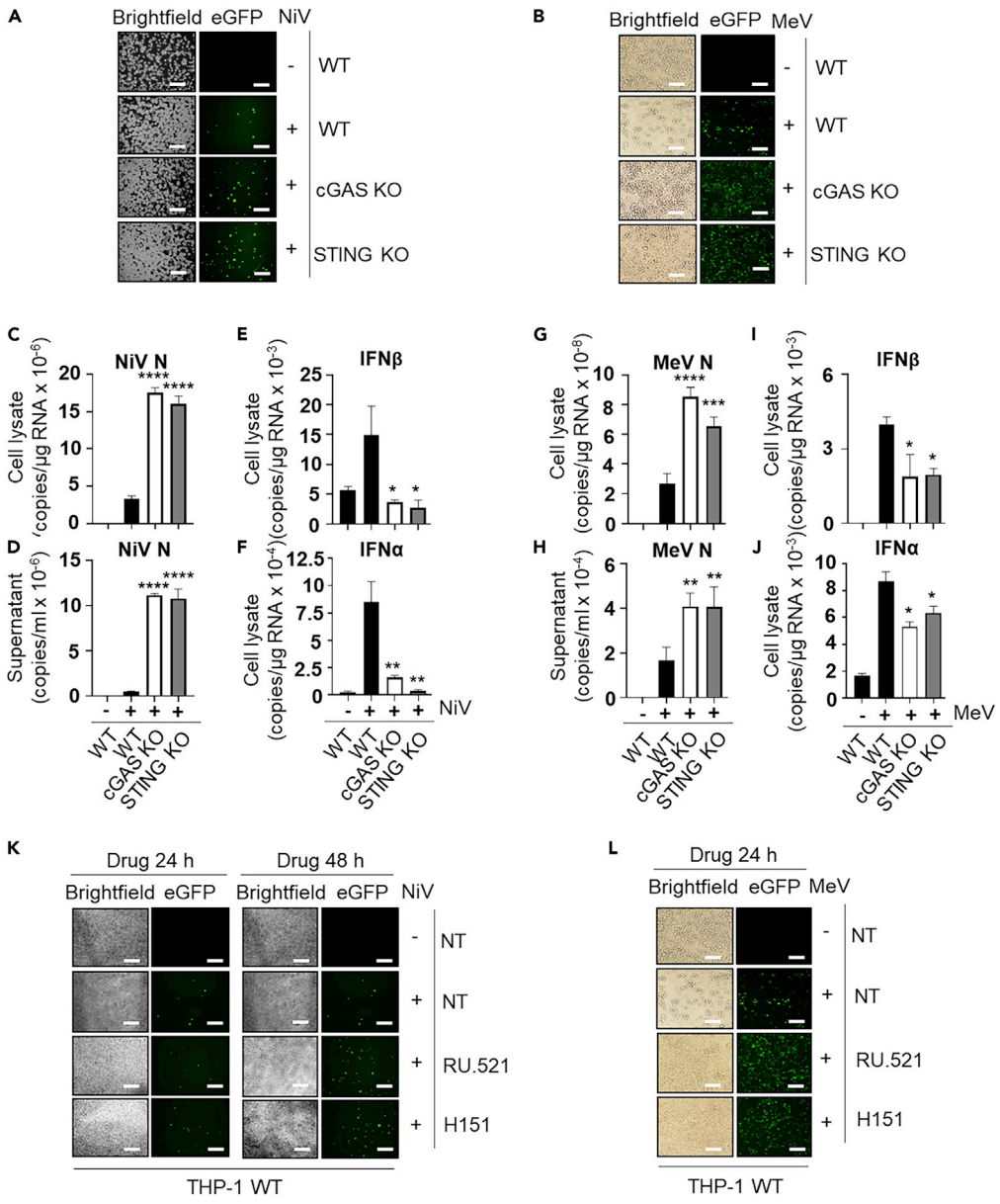

Figure 3. cGAS/STING pathway has a critical role in the control of paramyxovirus infection in human THP-1 cells

THP-1 cells deficient in the indicated signaling pathways were infected with NiV-eGFP and MeV-eGFP (MOI of 0.1) for 48 and 24 h respectively.

(A and B) Cells were analyzed for eGFP expression by fluorescence microscopy.

(C–J) Cell lysates and/or supernatants were harvested and analyzed by RT-qPCR for the expression of NiV-N (C and D), MeV-N (G and H), IFNβ (E and I), and IFNα (F and J). Data are represented as mean ± SEM. THP-1 WT cells treated or not (NT) with the specific inhibitors for cGAS (RU.521) or STING (H151) were infected with NiV-eGFP and MeV-eGFP (MOI of 0.1) for 24 and 48 h

(K and L) Cells were analyzed for eGFP expression by fluorescence microscopy. Scale bars, 100 µm. The statistical significance of differences between infected WT and KO cells was analyzed using one-way analysis of variance, followed by the Tukey multiple comparisons test. *$p < 0.05$; **$p < 0.01$; ***$p < 0.001$; ****$p < 0.0001$ compared with infected WT condition.

MeV receptors CD150 and Nectin 4 (Crimeen-Irwin et al., 2003; Noyce et al., 2011; Tatsuo et al., 2000). THP-1 cells depleted of cGAS or STING exhibited enhanced permissiveness to NiV and MeV infections when compared with their WT counterparts (Figures 3A, 3B, S2A, and S2B). This was analyzed by

fluorescence imaging of NiV propagation throughout cell cultures (Figure 3A), by the proportions of THP-1-infected cells as determined by flow cytometry (Figure S2A), and by the quantification of viral N RNA by RT-qPCR both in cell extracts (Figure 3C) and cell supernatants (Figure 3D). Correlatively, and in agreement with observations made in pMEFs infected with NiV, the higher permissiveness of cGAS KO and STING KO THP-1 cells was associated with the abolition of IFNβ and/or IFNα mRNA accumulations (Figures 3E and 3F). Comparable results were obtained after infection by MeV, although a reduced but significant accumulation of both IFNβ and IFNα mRNA was still observed in cGAS KO and STING KO cells (Figures 3G–3J).

As an alternative and complementary approach, we analyzed the paramyxoviral propagation within WT THP-1 cells treated with selective inhibitors of cGAS and STING, namely, RU-521 and H151, respectively. RU.521 is a competitive inhibitor of ATP and GTP substrates for binding to the cGAS catalytic pocket that prevents their cyclization into cGAMP (Vincent et al., 2017; Xie et al., 2019). H151 covalently binds to STING Cys91 and inhibits palmitoylation of STING and consequently the activation of IFN-I production (Haag et al., 2018). Addition of RU-521 or H151 1 h before infection resulted in an improved propagation of both NiV and MeV as evidenced by fluorescence microscopy (Figures 3K and 3L) and flow cytometry (Figures S2C–S2E).

Thus, the cGAS/STING axis appears to play a critical role in human cells to control paramyxovirus infections by allowing expression of IFNβ and to a lower extent of IFNα.

Paramyxovirus infection activates the cGAS/STING pathway in both murine and human cells

The increased viral infection observed upon abolition of either cGAS or STING suggested that paramyxoviruses could activate STING. This was investigated by analyzing specific phosphorylation and/or ubiquitination of activated STING in pMEFs, THP-1, and human pulmonary microvascular endothelial cells (HPMEC) as representative of primary targets of NiV infection in humans (Figures 4 and S3). A time course follow-up of the activation of cGAS/STING axis induced by viral infection was performed at 6, 24, and 48 h post-infection (hpi) by western blot using antibodies against STING-S366^{P} (Chiang and Gack, 2017). The expression level of STING remained unchanged throughout the 48h observation, whereas moderate amounts of STING-S366^{P} became detectable at 24 hpi and further increased at 48 hpi after NiV or MeV infection of HPMECs (Figures 4A and 4B) and THP-1 cells (Figures 4C and S3A). Importantly, STING-S366^{P} was not detected in NiV- or MeV-infected cGAS KO THP-1 cells at 24 and 48 hpi, and as expected in STING KO THP-1 cells (Figures 4C and S3A). Accordingly, STING-S366^{P} was also not detected in THP-1 cells infected and treated with either RU-521 or H151 (Figure S3A).

Accordingly, whereas uninfected WT pMEFs, NiV-infected STING KO, and MyD88/TRIF/MAVS/STING KO cells did not elicit any mouse STING-S365^{P} band (Tsuchiya et al., 2016), NiV-infected WT and MyD88/TRIF/MAVS KO pMEFs displayed activation of STING protein (Figure S3B). Importantly, the detection of the STING-S365^{P} band in MyD88/TRIF/MAVS KO pMEFs indicates that NiV infection activates the STING signaling pathway independently from the TLR-MyD88/TRIF and RLR/MAVS pathways of innate immunity. As K63-linked ubiquitination (Ub-K63) is another hallmark of STING activation, mainly associated with the activation of NF-κB (Chiang and Gack, 2017), STING ubiquitination was also evaluated in HPMECs infected for 48 h with NiV or MeV. Immunoprecipitated STING using anti-STING antibodies was found to be labeled by either anti-STING-S366P and anti-Ub-K63 antibodies through single phosphorylation or ubiquitination (Figures 4D and 4E) or K63 polyubiquitinations (Figure S3C) as described previously (Prabakaran et al., 2018; Zhang et al., 2012). As an apoptotic environment could activate STING in bystander cells (Ahn et al., 2012), a potential effect of virus-induced cell death in infected cultures was evaluated by analyzing caspase 3 activity. The levels of cleaved caspase 3 were minimally increased between uninfected and NiV- or MeV-infected cells, indicating that cell death had likely a minor impact on STING activation until 48 h post-infection (Figures 4A–4C, S3A, S3D, and S3E).

We conclude that negative-strand RNA paramyxoviruses activate the cGAS/STING axis to trigger the innate immune responses.

DISCUSSION

Although its role in response to DNA virus infection has been well deciphered (Eaglesham and Kranzusch, 2020), the role of cGAS/STING axis against RNA viruses such as paramyxoviruses is poorly understood. While cGAS was reported to interact with dsRNA, no production of cGAMP was detected, thus cGAS could not canonically activate STING directly (Civril et al., 2013). However, previous studies have shown interactions between RNA viruses and cGAS/STING in (1) their control by innate immunity or (2) their capacity to

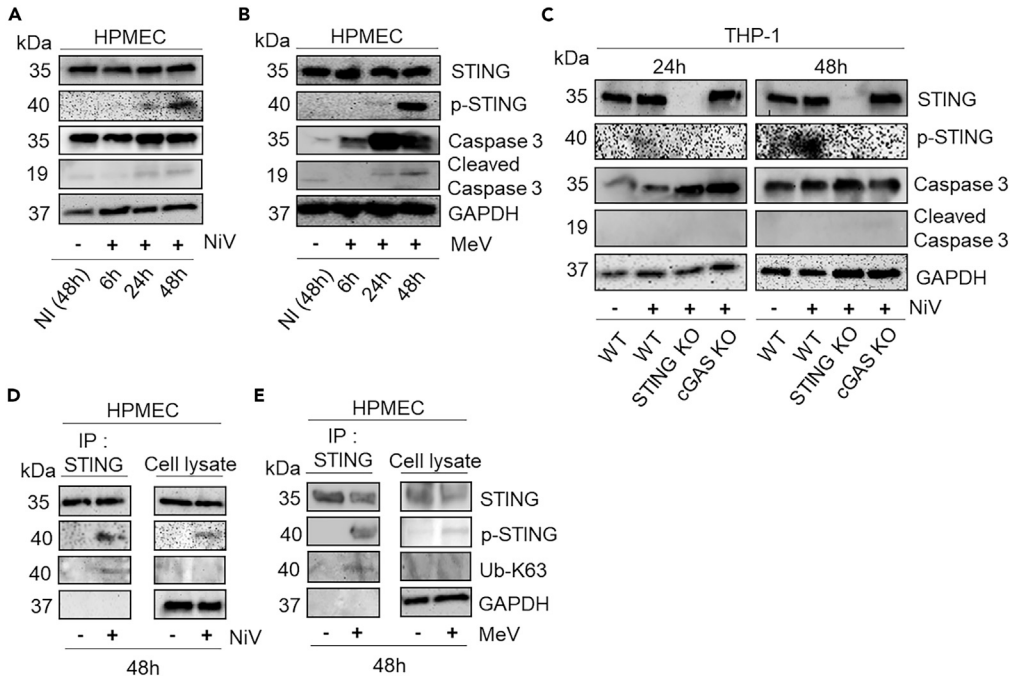

Figure 4. Paramyxovirus infection activates the cGAS/STING pathway in human cells

Human pulmonary microvascular endothelial (HPMEC) cells and THP-1 cells deficient in the indicated signaling platforms were infected with either NiV or MeV (MOI of 1) for 6, 24, or 48 h

(A–C) Cells were analyzed for phospho-STING (p-STING), STING, Caspase 3, cleaved Caspase 3, and GAPDH expression by western blot analysis.

(D and E) HPMEC cells were infected with NiV (D) and MeV (E) (MOI of 1) for 48 h before cell lysis. Endogenous STING was immunoprecipitated using anti-STING antibodies followed by western blot analyses using anti-STING, anti-Ub-K63, anti p-STING, and anti-GAPDH antibodies. In parallel, endogenous expression levels of STING, p-STING, and Ub-K63 together as GAPDH as loading control in cell lysates were analyzed by western blot. Shown data are representative of three independent experiments showing similar results.

See also Figure S3C for western blot showing multiple ubiquitination forms of STING.

disrupt the cGAS/STING pathway, reflecting a likely role of STING in host response (Aguirre et al., 2017; Franz et al., 2018; Ishikawa et al., 2009; Schoggins et al., 2014).

Paramyxoviruses replicate within the cytoplasm using their own RNA-dependent RNA polymerase, i.e., their replicative cycle does not rely on a DNA intermediate step (Gerlier and Lyles, 2011). As cGAS is exclusively activated upon binding to dsDNA (Kranzusch et al., 2013; Sun et al., 2013) or DNA/RNA hybrid (Mankan et al., 2014), we have to speculate about the identity of the cGAS agonist during infection by paramyxoviruses. Our experiments suggest that apoptosis is not involved in the mechanism of activation of the cGAS/STING pathway as caspase 3 activity remains undetected following NiV and MeV infections. As apoptotic caspases have been described to suppress mitochondrial-induced STING-mediated IFN-I production (White et al., 2014), we cannot exclude additional unknown mechanisms leading to the release of the mitochondrial DNA at some stage of viral infection, as evidenced after infection with dengue virus, a positive-stranded RNA virus (Aguirre et al., 2017; Sun et al., 2017). Furthermore, from observations made with Sendai virus, another paramyxovirus, possible virus-induced necroptosis appears unlikely to provoke STING activation (Schock et al., 2017). Finally, the role of viral-induced formation of syncytia remains to be explored because mechanical and bacterial induced cell-cell fusion has been reported to activate cGAS/STING pathway (Ku et al., 2020). Although the coexpression of MeV H and F glycoproteins did not result in the activation of IFN-I per se (Herschke et al., 2007), we cannot exclude a contribution of cell-cell fusion as a potential amplifier of cGAS/STING activation.

Collectively, the obtained data fit with a model where the infection by NiV or MeV activates cGAS/STING pathway. This activation results in the induction of the *IFNβ* and possibly the *IFNα* genes (see below) that

mediate the activation of an efficient antiviral program in *in vitro* and *in vivo* mouse models and/or in human cells closely mimicking what happens after the infection by mouse cytomegalovirus, a DNA virus (Tegtmeyer et al., 2019). Notably, the comparison of the triple and quadruple KO pMEFs indicate that cGAS/STING pathway strongly reinforces (or even conditions) the activation of type I IFN responses via the TLR8/MyD88 and/or the RLR/MAVS pathways by paramyxoviruses, including MeV (Ikegame et al., 2010; Runge et al., 2014; Seth et al., 2005).

STING can bind to RIG-I and MAVS (Sun et al., 2012) and is thought to potentiate the RLR/MAVS signaling leading to the activation of type I IFN (Ishikawa et al., 2009; Zevini et al., 2017; Zhong et al., 2008). The present data fit with this model. The defect of cGAS/STING pathway strongly facilitates the replication of both NiV and MeV as expected from the observed loss in activating IFN-I response. We cannot exclude that this facilitation results also from the concomitant disappearance of a STING-dependent inhibition of the translation of viral proteins as recently reported (Franz et al., 2018). However, they reported that the absence of STING modestly affects IFN response by negative-stranded RNA viruses infections compared with the present work.

Upon infection of MeV and/or NiV in mouse and/or human cells, the absence of cGAS/STING pathway affects IFNβ response and to a lower and more variable extent IFNα response. Owing to cell-dependent ability to produce IFNα, a different outcome may reflect higher expression of IRF-7 in pMEFs (Sharma et al., 2019) compared with THP-1 cells (Green et al., 2020). Indeed, whereas activation of the *IFNβ* gene optimally relies on IRF3 homodimers or IRF3/IRF7 heterodimers and NF-κB (Honda et al., 2005; Wathelet et al., 1998), the one for *IFNα* genes relies mostly relies on IRF7 homodimers (Yeow et al., 2000). Interestingly, STING mostly targets IRF-3 (Zhong et al., 2008) and NF-κB (Stempel et al., 2019) and consequently preferentially favors IFNβ.

Our study demonstrates that STING is activated against RNA viruses as also recently reported with SARS-CoV-2 (Neufeldt et al., 2020) and highlights that STING is modified and activated through S366 phosphorylation and/or K-63-linked ubiquitination during both NiV and MeV infections. Additional studies will uncover the occurrence of potential additional PTMs, STING subcellular location, and the source of the cognate DNA that activate cGAS during RNA virus infection.

In conclusion, cGAS/STING activation occurs during paramyxovirus infections, both *in vitro* and *in vivo*. This highlights an undefined aspect of the immune regulation against negative-strand viruses and reveals cGAS/STING as potential targets in the development of novel antiviral strategies.

Limitations of the study

Although mice are not the natural host of NiV and MeV infections, they provide numerous genetic tools to study their respective innate immune control. Further validation of the obtained results in human cell types or in a nonhuman primate model may allow overcoming the limitation of the murine model. Additional analysis of the role of cGAS/STING axis in the production of inflammatory cytokines will have to be performed. Furthermore, as the study of NiV requires the strict application of the BSL4 biosafety rules from the P4 Jean Mérieux laboratory in handling and inactivation of the samples, resulting in over-dilutions of the biological material in our co-immunoprecipitation and western blot experiments, there is a certain limit in the accurate detection of specific cellular or viral processes. Additional development of methodology and adjustments may be needed to study further the mechanisms, and the reproduction of similar results in MeV infection, requiring only BSL2 conditions, could overcome this limitation.

STAR★METHODS

Detailed methods are provided in the online version of this paper and include the following:

- KEY RESOURCES TABLE
- RESOURCE AVAILABILITY
  - Lead contact
  - Materials availability
  - Data and code availability
- EXPERIMENTAL MODEL AND SUBJECT DETAILS
  - Mice
  - Cell lines
  - Ethical statement

SUPPLEMENTAL INFORMATION

Supplemental information can be found online at https://doi.org/10.1016/j.isci.2021.102519.

ACKNOWLEDGMENTS

The work was supported by INSERM, LABEX ECOFECT (ANR-11-LABX-0048) of Lyon University, within the program "Investissements d'Avenir" (ANR-11-IDEX-0007) operated by the French National Research Agency (ANR), by ANR-18-CE11-0014-02, by Aviesan Sino-French agreement on Nipah virus study, and by the Deutsche Forschungsgemeinschaft (DFG, German Research Foundation), SFB900/3 B2, project number 158989968, and the Joint French-German Project cGASVAC, project number 406922110. We thank the entire animal experimentation team of INSERM "Jean Mérieux" BSL4 laboratory for the realization of the animal experiment and the biosafety team for their assistance for BSL4 activities. We are grateful to all the members of the group Immunobiology of viral infection at CIRI, for the help in the realization of this study. We acknowledge the contribution of the SFR Biosciences (UMS3444/CNRS, US8/INSERM, ENS de Lyon, UCBL) flow cytometry facility.

AUTHOR CONTRIBUTIONS

M.I., U.K., and B.H. designed the study. M.I., C.D., C.M., J.R., A.C., S.D., K.P.D., N.A., and S.M. performed experiments. M.I., C.M., J.S., D.G., and B.H. analyzed the data. M.I., J.S., D.G., and B.H. wrote the article. M.I., J.S., D.G., and B.H. prepared the figures. M.F., R.P., J.S., and U.K. provided some essential tools.

DECLARATION OF INTERESTS

The authors declare no competing interests.

Received: January 22, 2021
Revised: April 2, 2021
Accepted: May 5, 2021
Published: June 25, 2021

REFERENCES

Adachi, O., Kawai, T., Takeda, K., Matsumoto, M., Tsutsui, H., Sakagami, M., Nakanishi, K., and Akira, S. (1998). Targeted disruption of the MyD88 gene results in loss of IL-1- and IL-18-mediated function. Immunity *9*, 143–150.

Aguirre, S., Luthra, P., Sanchez-Aparicio, M.T., Maestre, A.M., Patel, J., Lamothe, F., Fredericks, A.C., Tripathi, S., Zhu, T., Pintado-Silva, J., et al. (2017). Dengue virus NS2B protein targets cGAS for degradation and prevents mitochondrial DNA sensing during infection. Nat. Microbiol. *2*, 17037.

Ahn, J., Gutman, D., Saijo, S., and Barber, G.N. (2012). STING manifests self DNA-dependent inflammatory disease. Proc. Natl. Acad. Sci. *109*, 19386–19391.

Akira, S., Uematsu, S., and Takeuchi, O. (2006). Pathogen recognition and innate immunity. Cell *124*, 783–801.

Baccala, R., Gonzalez-Quintial, R., Lawson, B.R., Stern, M.E., Kono, D.H., Beutler, B., and Theofilopoulos, A.N. (2009). Sensors of the innate immune system: their mode of action. Nat. Rev. Rheumatol. *5*, 448–456.

Borden, E.C., Sen, G.C., Uze, G., Silverman, R.H., Ransohoff, R.M., Foster, G.R., and Stark, G.R. (2007). Interferons at age 50: past, current and future impact on biomedicine. Nat. Rev. Drug Discov. *6*, 975–990.

Brune, W., Hengel, H., and Koszinowski, U.H. (2001). A mouse model for cytomegalovirus infection. Curr. Protoc. Immunol. *19*, 19.7.

Bustin, S.A., Benes, V., Garson, J.A., Hellemans, J., Huggett, J., Kubista, M., Mueller, R., Nolan, T., Pfaffl, M.W., Shipley, G.L., et al. (2009). The MIQE guidelines: minimum information for publication of quantitative real-time PCR experiments. Clin. Chem. *55*, 611–622.

Chang, D., Whiteley, A.T., Bugda Gwilt, K., Lencer, W.I., Mekalanos, J.J., and Thiagarajah,

J.R. (2020). Extracellular cyclic dinucleotides induce polarized responses in barrier epithelial cells by adenosine signaling. Proc. Natl. Acad. Sci. U S A *117*, 27502–27508.

Chiang, C., and Gack, M.U. (2017). Post-translational control of intracellular pathogen sensing pathways. Trends Immunol. *38*, 39–52.

Civril, F., Deimling, T., de Oliveira Mann, C.C., Ablasser, A., Moldt, M., Witte, G., Hornung, V., and Hopfner, K.-P. (2013). Structural mechanism of cytosolic DNA sensing by cGAS. Nature *498*, 332–337.

Cong, X., Yuan, Z., Du, Y., Wu, B., Lu, D., Wu, X., Zhang, Y., Li, F., Wei, B., Li, J., et al. (2019). Crystal structures of porcine STING ^{CBD} –CDN complexes reveal the mechanism of ligand recognition and discrimination of STING proteins. J. Biol. Chem. *294*, 11420–11432.

Crimeen-Irwin, B., Ellis, S., Christiansen, D., Ludford-Menting, M.J., Milland, J., Lanteri, M., Loveland, B.E., Gerlier, D., and Russell, S.M. (2003). Ligand binding determines whether CD46 is internalized by clathrin-coated pits or macropinocytosis. J. Biol. Chem. *278*, 46927–46937.

Der, S.D., Zhou, A., Williams, B.R., and Silverman, R.H. (1998). Identification of genes differentially regulated by interferon alpha, beta, or gamma using oligonucleotide arrays. Proc. Natl. Acad. Sci. U S A *95*, 15623–15628.

Dhondt, K.P., Mathieu, C., Chalons, M., Reynaud, J.M., Vallve, A., Raoul, H., and Horvat, B. (2013). Type I interferon signaling protects mice from lethal henipavirus infection. J. Infect. Dis. *207*, 142–151.

Dobbs, N., Burnaevskiy, N., Chen, D., Gonugunta, V.K., Alto, N.M., and Yan, N. (2015). STING activation by translocation from the ER is associated with infection and autoinflammatory disease. Cell Host Microbe *18*, 157–168.

Eaglesham, J.B., and Kranzusch, P.J. (2020). Conserved strategies for pathogen evasion of cGAS-STING immunity. Curr. Opin. Immunol. *66*, 27–34.

Ergun, S.L., Fernandez, D., Weiss, T.M., and Li, L. (2019). STING polymer structure reveals mechanisms for activation, hyperactivation, and inhibition. Cell *178*, 290–301.e10.

Ferren, M., Horvat, B., and Mathieu, C. (2019). Measles encephalitis: towards new therapeutics. Viruses *11*, 1017.

Franz, K.M., Neidermyer, W.J., Tan, Y.-J., Whelan, S.P.J., and Kagan, J.C. (2018). STING-dependent translation inhibition restricts RNA virus replication. Proc. Natl. Acad. Sci. U S A *115*, E2058–E2067.

Gao, P., Ascano, M., Wu, Y., Barchet, W., Gaffney, B.L., Zillinger, T., Serganov, A.A., Liu, Y., Jones, R.A., Hartmann, G., et al. (2013). Cyclic [G(2′,5′) pA(3′,5′)p] is the metazoan second messenger produced by DNA-activated cyclic GMP-AMP synthase. Cell *153*, 1094–1107.

Gerlier, D., and Lyles, D.S. (2011). Interplay between innate immunity and negative-strand RNA viruses: towards a rational model. Microbiol. Mol. Biol. Rev. *75*, 468–490.

Green, I.D., Pinello, N., Song, R., Lee, Q., Halstead, J.M., Kwok, C.-T., Wong, A.C.H., Nair, S.S., Clark, S.J., Roediger, B., et al. (2020). Macrophage development and activation involve coordinated intron retention in key inflammatory regulators. Nucleic Acids Res. *48*, 6513–6529.

Gui, X., Yang, H., Li, T., Tan, X., Shi, P., Li, M., Du, F., and Chen, Z.J. (2019). Autophagy induction via STING trafficking is a primordial function of the cGAS pathway. Nature *567*, 262–266.

Haag, S.M., Gulen, M.F., Reymond, L., Gibelin, A., Abrami, L., Decout, A., Heymann, M., van der Goot, F.G., Turcatti, G., Behrendt, R., et al. (2018). Targeting STING with covalent small-molecule inhibitors. Nature *559*, 269–273.

Hashimoto, K., Ono, N., Tatsuo, H., Minagawa, H., Takeda, M., Takeuchi, K., and Yanagi, Y. (2002). SLAM (CD150)-independent measles virus entry as revealed by recombinant virus expressing green fluorescent protein. J. Virol. *76*, 6743–6749.

Hayden, L., Semenoff, T., Schultz, V., Merz, S.F., Chapple, K.J., Rodriguez, M., Warrington, A.E., Shi, X., McKimmie, C.S., Edgar, J.M., et al. (2020). Lipid-specific IgMs induce antiviral responses in the CNS: implications for progressive multifocal leukoencephalopathy in multiple sclerosis. Acta Neuropathol. Commun. *8*, 135.

Herschke, F., Plumet, S., Duhen, T., Azocar, O., Druelle, J., Laine, D., Wild, T.F., Rabourdin-Combe, C., Gerlier, D., and Valentin, H. (2007). Cell-cell fusion induced by measles virus amplifies the type I interferon response. J. Virol. *81*, 12859–12871.

Honda, K., Yanai, H., Negishi, H., Asagiri, M., Sato, M., Mizutani, T., Shimada, N., Ohba, Y., Takaoka, A., Yoshida, N., et al. (2005). IRF-7 is the master regulator of type-I interferon-dependent immune responses. Nature *434*, 772–777.

Iampietro, M., Aurine, N., Dhondt, K.P., Dumont, C., Pelissier, R., Spanier, J., Vallve, A., Raoul, H., Kalinke, U., and Horvat, B. (2020). Control of Nipah virus infection in mice by the host adaptors mitochondrial antiviral signaling protein (MAVS) and myeloid differentiation primary response 88 (MyD88). J. Infect. Dis. *221*, S401–S406.

Ikegame, S., Takeda, M., Ohno, S., Nakatsu, Y., Nakanishi, Y., and Yanagi, Y. (2010). Both RIG-I and MDA5 RNA helicases contribute to the induction of alpha/beta interferon in measles virus-infected human cells. JVI *84*, 372–379.

Ishikawa, H., and Barber, G.N. (2008). STING is an endoplasmic reticulum adaptor that facilitates innate immune signalling. Nature *455*, 674–678.

Ishikawa, H., Ma, Z., and Barber, G.N. (2009). STING regulates intracellular DNA-mediated, type I interferon-dependent innate immunity. Nature *461*, 788–792.

Kranzusch, P.J., Lee, A.S.-Y., Berger, J.M., and Doudna, J.A. (2013). Structure of human cGAS reveals a conserved family of second-messenger enzymes in innate immunity. Cell Rep. *3*, 1362–1368.

Kranzusch, P.J., Lee, A.S.Y., Wilson, S.C., Solovykh, M.S., Vance, R.E., Berger, J.M., and Doudna, J.A. (2014). Structure-guided reprogramming of human cGAS dinucleotide linkage specificity. Cell *158*, 1011–1021.

Krump-Konvalinkova, V., Bittinger, F., Unger, R.E., Peters, K., Lehr, H.A., and Kirkpatrick, C.J. (2001). Generation of human pulmonary microvascular endothelial cell lines. Lab Invest. *81*, 1717–1727.

Ku, J.W.K., Chen, Y., Lim, B.J.W., Gasser, S., Crasta, K.C., and Gan, Y.-H. (2020). Bacterial-induced cell fusion is a danger signal triggering cGAS–STING pathway via micronuclei formation. Proc. Natl. Acad. Sci. U S A *117*, 15923–15934.

Liu, S., Cai, X., Wu, J., Cong, Q., Chen, X., Li, T., Du, F., Ren, J., Wu, Y.-T., Grishin, N.V., et al. (2015). Phosphorylation of innate immune adaptor proteins MAVS, STING, and TRIF induces IRF3 activation. Science *347*, aaa2630.

Mankan, A.K., Schmidt, T., Chauhan, D., Goldeck, M., Höning, K., Gaidt, M., Kubarenko, A.V., Andreeva, L., Hopfner, K., and Hornung, V. (2014). Cytosolic RNA:DNA hybrids activate the cGAS –STING axis. EMBO J. *33*, 2937–2946.

Mathieu, C., Guillaume, V., Volchkova, V.A., Pohl, C., Jacquot, F., Looi, R.Y., Wong, K.T., Legras-Lachuer, C., Volchkov, V.E., Lachuer, J., and Horvat, B. (2012). Nonstructural Nipah virus C protein regulates both the early host proinflammatory response and viral virulence. J. Virol. https://doi.org/10.1128/JVI.01203-12.

Mathieu, C., Pohl, C., Szecsi, J., Trajkovic-Bodennec, S., Devergnas, S., Raoul, H., Cosset, F.L., Gerlier, D., Wild, T.F., and Horvat, B. (2011). Nipah virus uses leukocytes for efficient dissemination within a host. J. Virol. https://doi.org/10.1128/JVI.00549-11.

Mehand, M.S., Al-Shorbaji, F., Millett, P., and Murgue, B. (2018). The WHO R&D Blueprint: 2018 review of emerging infectious diseases requiring urgent research and development efforts. Antiviral Res. *159*, 63–67.

Mogensen, T.H. (2009). Pathogen recognition and inflammatory signaling in innate immune defenses. Clin. Microbiol. Rev. *22*, 240–273.

Mukai, K., Konno, H., Akiba, T., Uemura, T., Waguri, S., Kobayashi, T., Barber, G.N., Arai, H., and Taguchi, T. (2016). Activation of STING requires palmitoylation at the Golgi. Nat. Commun. *7*, 11932.

Muller, U., Steinhoff, U., Reis, L.F., Hemmi, S., Pavlovic, J., Zinkernagel, R.M., and Aguet, M. (1994). Functional role of type I and type II interferons in antiviral defense. Science *264*, 1918–1921.

Naniche, D., Varior-Krishnan, G., Cervoni, F., Wild, T.F., Rossi, B., Rabourdin-Combe, C., and Gerlier, D. (1993). Human membrane cofactor protein (CD46) acts as a cellular receptor for measles virus. J. Virol. *67*, 6025–6032.

Neufeldt, C.J., Cerikan, B., Cortese, M., Frankish, J., Lee, J.-Y., Plociennikowska, A., Heigwer, F., Joecks, S., Burkart, S.S., Zander, D.Y., et al. (2020). SARS-CoV-2 Infection Induces a Pro-inflammatory Cytokine Response through cGAS-STING and NF-Kb (Microbiology).

Ni, G., Konno, H., and Barber, G.N. (2017). Ubiquitination of STING at lysine 224 controls IRF3 activation. Sci. Immunol. *2*, eaah7119.

Ni, G., Ma, Z., and Damania, B. (2018). cGAS and STING: at the intersection of DNA and RNA virus-sensing networks. PLoS Pathog. *14*, e1007148.

Noyce, R.S., Bondre, D.G., Ha, M.N., Lin, L.T., Sisson, G., Tsao, M.S., and Richardson, C.D. (2011). Tumor cell marker PVRL4 (nectin 4) is an epithelial cell receptor for measles virus. PLoS Pathog. *7*, e1002240.

Park, A., and Iwasaki, A. (2020). Type I and type III interferons - induction, signaling, evasion, and application to combat COVID-19. Cell Host Microbe *27*, 870–878.

Pelissier, R., Iampietro, M., and Horvat, B. (2019). Recent advances in the understanding of Nipah virus immunopathogenesis and anti-viral approaches. F1000Res *8*, 1763.

Pfaffl, M.W. (2001). A new mathematical model for relative quantification in real-time RT-PCR. Nucleic Acids Res. *29*, e45.

Prabakaran, T., Bodda, C., Krapp, C., Zhang, B.-C., Christensen, M.H., Sun, C., Reinert, L., Cai, Y., Jensen, S.B., Skouboe, M.K., et al. (2018). Attenuation of cGAS-STING signaling is mediated by a p62/SQSTM1-dependent autophagy pathway activated by TBK1. EMBO J. *37*, e97858.

Runge, S., Sparrer, K.M.J., Lässig, C., Hembach, K., Baum, A., García-Sastre, A., Söding, J., Conzelmann, K.-K., and Hopfner, K.-P. (2014). In vivo ligands of MDA5 and RIG-I in measles virus-infected cells. PLoS Pathog. *10*, e1004081.

Schock, S.N., Chandra, N.V., Sun, Y., Irie, T., Kitagawa, Y., Gotoh, B., Coscoy, L., and Winoto, A. (2017). Induction of necroptotic cell death by viral activation of the RIG-I or STING pathway. Cell Death Differ. *24*, 615–625.

Schoggins, J.W., MacDuff, D.A., Imanaka, N., Gainey, M.D., Shrestha, B., Eitson, J.L., Mar, K.B., Richardson, R.B., Ratushny, A.V., Litvak, V., et al. (2014). Pan-viral specificity of IFN-induced genes reveals new roles for cGAS in innate immunity. Nature *505*, 691–695.

Sen, G.C., and Peters, G.A. (2007). Viral stress-inducible genes. Adv. Virus Res. *70*, 233–263.

Seth, R.B., Sun, L., Ea, C.-K., and Chen, Z.J. (2005). Identification and characterization of MAVS, a mitochondrial antiviral signaling protein that activates NF-kappaB and IRF 3. Cell *122*, 669–682.

Shang, G., Zhu, D., Li, N., Zhang, J., Zhu, C., Lu, D., Liu, C., Yu, Q., Zhao, Y., Xu, S., et al. (2012). Crystal structures of STING protein reveal basis for recognition of cyclic di-GMP. Nat. Struct. Mol. Biol. *19*, 725–727.

Sharma, K.B., Sharma, M., Aggarwal, S., Yadav, A.K., Bhatnagar, S., Vrati, S., and Kalia, M. (2019). Quantitative proteome analysis of *Atg5* -deficient mouse embryonic fibroblasts reveals the range of the autophagy-modulated basal cellular proteome. MSystems *4*, e00481–19.

Soman Pillai, V., Krishna, G., and Valiya Veettil, M. (2020). Nipah virus: past outbreaks and future containment. Viruses *12*, 465.

Spanier, J., Lienenklaus, S., Paijo, J., Kessler, A., Borst, K., Heindorf, S., Baker, D.P., Kröger, A., Weiss, S., Detje, C.N., et al. (2014). Concomitant TLR/RLH signaling of radioresistant and radiosensitive cells is essential for protection against vesicular stomatitis virus infection. J. Immunol. *193*, 3045–3054.

Stempel, M., Chan, B., Juranić Lisnić, V., Krmpotić, A., Hartung, J., Paludan, S.R., Füllbrunn, N., Lemmermann, N.A., and Brinkmann, M.M. (2019). The herpesviral antagonist m152 reveals differential activation of STING -dependent IRF and NF -κB signaling and STING 's dual role during MCMV infection. EMBO J. *38*, e100983.

Sun, B., Sundström, K.B., Chew, J.J., Bist, P., Gan, E.S., Tan, H.C., Goh, K.C., Chawla, T., Tang, C.K., and Ooi, E.E. (2017). Dengue virus activates cGAS through the release of mitochondrial DNA. Sci. Rep. *7*, 3594.

Sun, L., Xing, Y., Chen, X., Zheng, Y., Yang, Y., Nichols, D.B., Clementz, M.A., Banach, B.S., Li, K., Baker, S.C., et al. (2012). Coronavirus papain-like proteases negatively regulate antiviral innate immune response through disruption of STING-mediated signaling. PLoS One *7*, e30802.

Sun, L., Wu, J., Du, F., Chen, X., and Chen, Z.J. (2013). Cyclic GMP-AMP synthase is a cytosolic DNA sensor that activates the type I interferon pathway. Science *339*, 786–791.

Tanaka, Y., and Chen, Z.J. (2012). STING specifies IRF3 phosphorylation by TBK1 in the cytosolic DNA signaling pathway. Sci. Signal. *5*, ra20.

Tatsuo, H., Ono, N., Tanaka, K., and Yanagi, Y. (2000). SLAM (CDw150) is a cellular receptor for measles virus. Nature *406*, 893–897.

Tegtmeyer, P.-K., Spanier, J., Borst, K., Becker, J., Riedl, A., Hirche, C., Ghita, L., Skerra, J., Baumann, K., Lienenklaus, S., et al. (2019). STING induces early IFN-β in the liver and constrains myeloid cell-mediated dissemination of murine cytomegalovirus. Nat. Commun. *10*, 2830.

Thibault, P.A., Watkinson, R.E., Moreira-Soto, A., Drexler, J.F., and Lee, B. (2017). Zoonotic potential of emerging paramyxoviruses: knowns and unknowns. Adv. Virus Res. *98*, 1–55.

Tsuchiya, Y., Jounai, N., Takeshita, F., Ishii, K.J., and Mizuguchi, K. (2016). Ligand-induced ordering of the C-terminal tail primes STING for phosphorylation by TBK1. EBioMedicine *9*, 87–96.

Vincent, J., Adura, C., Gao, P., Luz, A., Lama, L., Asano, Y., Okamoto, R., Imaeda, T., Aida, J., Rothamel, K., et al. (2017). Small molecule inhibition of cGAS reduces interferon expression in primary macrophages from autoimmune mice. Nat. Commun. *8*, 750.

Waibler, Z., Anzaghe, M., Ludwig, H., Akira, S., Weiss, S., Sutter, G., and Kalinke, U. (2007). Modified vaccinia virus Ankara induces Toll-like receptor-independent type I interferon responses. J. Virol. *81*, 12102–12110.

Wathelet, M.G., Lin, C.H., Parekh, B.S., Ronco, L.V., Howley, P.M., and Maniatis, T. (1998). Virus infection induces the assembly of coordinately activated transcription factors on the IFN-β enhancer in vivo. Mol. Cell *1*, 507–518.

Welsch, J.C., Talekar, A., Mathieu, C., Pessi, A., Moscona, A., Horvat, B., and Porotto, M. (2013). Fatal measles virus infection prevented by brain-penetrant fusion inhibitors. J. Virol. https://doi.org/10.1128/JVI.02436-13.

Wesche, H., Henzel, W.J., Shillinglaw, W., Li, S., and Cao, Z. (1997). MyD88: an adapter that recruits IRAK to the IL-1 receptor complex. Immunity *7*, 837–847.

White, M.J., McArthur, K., Metcalf, D., Lane, R.M., Cambier, J.C., Herold, M.J., van Delft, M.F., Bedoui, S., Lessene, G., Ritchie, M.E., et al. (2014). Apoptotic caspases suppress mtDNA-induced STING-mediated type I IFN production. Cell *159*, 1549–1562.

Xie, W., Lama, L., Adura, C., Tomita, D., Glickman, J.F., Tuschl, T., and Patel, D.J. (2019). Human cGAS catalytic domain has an additional DNA-binding interface that enhances enzymatic activity and liquid-phase condensation. Proc. Natl. Acad. Sci. U S A *116*, 11946–11955.

Yamamoto, M., Sato, S., Hemmi, H., Hoshino, K., Kaisho, T., Sanjo, H., Takeuchi, O., Sugiyama, M., Okabe, M., Takeda, K., et al. (2003). Role of adaptor TRIF in the MyD88-independent toll-like receptor signaling pathway. Science *301*, 640–643.

Yeow, W.-S., Au, W.-C., Juang, Y.-T., Fields, C.D., Dent, C.L., Gewert, D.R., and Pitha, P.M. (2000). Reconstitution of virus-mediated expression of interferon α genes in human fibroblast cells by ectopic interferon regulatory factor-7. J. Biol. Chem. *275*, 6313–6320.

Yoneda, M., Guillaume, V., Ikeda, F., Sakuma, Y., Sato, H., Wild, T.F., and Kai, C. (2006). Establishment of a Nipah virus rescue system. Proc. Natl. Acad. Sci. U S A *103*, 16508–16513.

Zevini, A., Olagnier, D., and Hiscott, J. (2017). Crosstalk between cytoplasmic RIG-I and STING sensing pathways. Trends Immunol. *38*, 194–205.

Zhang, J., Hu, M.-M., Wang, Y.-Y., and Shu, H.-B. (2012). TRIM32 protein modulates type I interferon induction and cellular antiviral response by targeting MITA/STING protein for K63-linked ubiquitination. J. Biol. Chem. *287*, 28646–28655.

Zhang, X., Wu, J., Du, F., Xu, H., Sun, L., Chen, Z., Brautigam, C.A., Zhang, X., and Chen, Z.J. (2014). The cytosolic DNA sensor cGAS forms an oligomeric complex with DNA and undergoes switch-like conformational changes in the activation loop. Cell Rep. *6*, 421–430.

Zhong, B., Yang, Y., Li, S., Wang, Y.-Y., Li, Y., Diao, F., Lei, C., He, X., Zhang, L., Tien, P., et al. (2008). The adaptor protein MITA links virus-sensing receptors to IRF3 transcription factor activation. Immunity *29*, 538–550.

STAR★METHODS

KEY RESOURCES TABLE

REAGENT or RESOURCE	SOURCE	IDENTIFIER
Antibodies		
Horseradish peroxydase conjugated anti-mouse IgG antibody	Promega	Cat# W4021
Horseradish peroxydase conjugated anti-rabbit IgG antibody	Promega	Cat# W4011
Mouse anti-GAPDH antibody	Chemicon	Cat# MAB374
Mouse anti-human Ub-K63 antibody	eBioscience	Cat# 14-6077-82
Rabbit anti-Caspase 3 antibody	Cell Signaling	Cat# 9662S
Rabbit anti-cleaved Caspase 3 antibody	Cell Signaling	Cat# 9661S
Rabbit anti-human S366 p-STING antibody	Cell Signaling	Cat# 19781S
Rabbit anti-mouse S365 p-STING antibody	Cell Signaling	Cat# 72971S
Rabbit anti-NiV N antibody	Valbex	Dhondt et al., (2013)
Rabbit anti-STING antibody	Cell Signaling	Cat# 13647S
Bacterial and virus strains		
Nipah virus (NiV) Malaysia strain UMMC1	University of Malaya	GenBank AY029767
rMeV-EdmH-eGFP	CIRI BSL2, Lyon	Hashimoto et al., (2002)
rNiV-eGFP	INSERM Jean Mérieux BSL4, Lyon	Yoneda et al., (2006)
Chemicals, peptides, and recombinant proteins		
Cocktail of protease inhibitor	Thermo Scientific	Cat# 78444
Complete protease inhibitor 1X	Roche	Cat# 11836145001
Epitope retrieval solution (Distilled water, 10mM sodium citrate, 0.05% Tween 20)	This paper	N/A
H-151	InvivoGen	Cat# inh-h151
Hydrogen Peroxyde 30%	Merck	Cat# 107209
Laemmli 4X	Life Technologies	Cat# NP0008
Modified Harris Solution Hematoxylin	Sigma Aldrich	Cat# HHS16
Protein A/G agarose beads	Pierce	Cat# 20421
Reducing agent 10X	Invitrogen	Cat# NP0009
RIPA Lysis buffer	Pierce	Cat# 89901
RU.521	InvivoGen	Cat# inh-ru521
Signal West Femto reagent	ThermoScientific	Cat# 34096
Sodium citrate	Sigma Aldrich	Cat# C8532
Super Signal West Dura	ThermoScientific	Cat# 34076
TBS 10X	Euromedex	Cat# ET220-B
Triton X-100	Sigma Aldrich	Cat# T8787

(*Continued on next page*)

Continued

REAGENT or RESOURCE	SOURCE	IDENTIFIER
Trypsin 0.25% EDTA	Gibco	Cat# 25200-056
Tween20	VWR	Cat# 28829.296
Xylene	VWR	Cat# 28975.291
Critical commercial assays		
ImmPRESS® HRP Anti-Rabbit IgG (Peroxidase)	LSBio	Cat# LS-J1066-15
iScript cDNA Synthesis Kit	Bio-Rad	Cat# 170-8891
MycoAlerte	Lonza	Cat# LT07-318
NucleoSpin RNA Kit	Macherey-Nagel	Cat# 740955.250
Platinum SYBR Green qPCR SuperMix-UDG	Invitrogen	Cat# 11744-500
Qiagen QIamp Viral RNA	Qiagen	Cat# 52906
Experimental models: Cell lines		
HPMEC	Krump-Konvalinkova et al., (2001)	N/A
MEFs	Brune et al., (2001)	N/A
THP-1	Mankan et al., (2014)	N/A
Experimental models: Organisms/strains		
C57BL/6 WT mice	Charles River	Cat# C57BL/6NCrl
C57BL/6 IFNAR KO mice	Muller et al. (1994)	N/A
C57BL/6 MyD88 KO mice	Adachi et al., (1998)	N/A
C57BL/6 MyD88/TRIF KO mice	Waibler et al., (2007)	N/A
C57BL/6 MyD88/TRIF/MAVS KO mice	Spanier et al., (2014)	N/A
C57BL/6 MyD88/TRIF/MAVS/STING KO mice	Tegtmeyer et al., (2019)	N/A
Oligonucleotides		
Human GAPDH For: CACCCACTCCTCCACCTTTGAC Rev: GTCCACCACCCTGTTGCTGTAG	Mathieu et al. (2011)	N/A
Human IFNα For: AGTCACCCATCTCAGCAAGCC Rev: ACCACCAGGACCATCAGTAAAGC	This paper	N/A
Human IFNβ For: CTCCTAGCCTGTGCCTCTGG Rev: TGCAGTACATTAGCCATCAGTCAC	This paper	N/A
MeV-N For: GTGATCAAAGTGAGAATGAGCT Rev: GCTGACCTTCGACTGTCCT	Welsch et al. (2013)	N/A
Mouse GAPDH For: GCATGGCCTTCCGTGTCC Rev: TGTCATCATACTTGGCAGGTTTCT	Mathieu et al. (2012)	N/A
Mouse IFNα For: CTCTGTGCTTTCCTGATG Rev: CCTGAGGTTATGAGTCTGA	Iampietro et al., (2020)	N/A
Mouse IFNβ For: TCCACTTGAAGAGCTATTAC Rev: CATTCTGAGGCATCAACT	Iampietro et al., (2020)	N/A

(*Continued on next page*)

Continued

REAGENT or RESOURCE	SOURCE	IDENTIFIER
NiV-N For: GGCAGGATTCTTCGCAACCATC Rev: GGCTCTTGGGCCAATTTCTCTG	Mathieu et al. (2011)	N/A
Software and algorithms		
FlowJo v.10	FlowJo	https://www.flowjo.com/solutions/flowjo/downloads
GraphPad Prism 8.3.0	GraphPad Software Inc.	https://www.graphpad.com/scientific-software/prism
ImageJ 1.52p FiJi package	Image J	https://imagej.net/Fiji
StepOnePlus v2.3	ThermoScientific	https://www.thermofisher
Beacon Designer (version 8)	Premier Biosoft	http://www.premierbiosoft.com/molecular_beacons/
Amplify	N/A	https://engels.genetics.wisc.edu/amplify/
Other		
4L Fortessa Flow cytometer	BD Biosciences	https://www.bdbiosciences.com/enin/instruments/researchinstruments/research-cellanalyzers/lsrfortessa
ChemiDoc Imaging System	Bio-Rad	https://www.bio-rad.com/frfr/product/chemidoc-imagingsystem?ID=OI91XQ15
DS-11-FX spectrophotometer	DeNovix	https://www.denovix.com
Eclipse Ts2R NIKON	Nikon	https://www.microscope.healthcare.nikon.com/products/invertedmicroscopes/eclipse-ts2r
Gallios Flow cytometer	Beckman Coulter	https://www.beckman.com/flowcytometry/instruments/gallios
StepOnePlus Real-Time PCR System	Applied Biosystems	https://www.thermofisher.com/fr/fr/home/life-science/pcr/realtime-pcr/real-time-pcr
VersaDoc Imaging System	Bio-Rad	http://www.biorad.com/webroot/web/pdf/lsr/literature/Bulletin_5609.pdf
Zeiss Axiovert 100M	Zeiss	https://www.zeiss.com/microscopy/int/products/lightmicroscopes/axio-vert-a1-forbiology.Html

RESOURCE AVAILABILITY

Lead contact

Information and requests for resources may be directed to and will be fulfilled by the lead contact Mathieu Iampietro (mathieu.iampietro@inserm.fr)

Materials availability

This study did not generate new unique reagents.

Data and code availability

No new data/code was generated in this study

EXPERIMENTAL MODEL AND SUBJECT DETAILS

Mice

Several lines of transgenic mice, all in C57BL/6 genetic background, were used: wild type (WT) C57BL/6J mice and following knockout (KO) models: mice deleted for IFN-I receptor (IFNAR-KO) (Muller et al., 1994), TLR adaptor protein MyD88 (MyD88-KO) (Adachi et al., 1998), and mice crossed to bear several deletions, including MyD88/TRIF-KO (Waibler et al., 2007), MyD88/TRIF/MAVS-KO (Spanier et al., 2014) and MyD88/TRIF/MAVS/STING KO (Tegtmeyer et al., 2019).

Cell lines

Primary murine embryonic fibroblasts (pMEFs) were isolated from murine embryos obtained from female pregnant mice 13 days after conception (Brune et al., 2001) and cultured in Dulbecco's modified Eagle's medium (DMEM) GlutaMAX supplemented with 10% heat-inactivated fetal bovine serum (FBS), 0.2% 2-mercaptoethanol, 1% HEPES, 1% nonessential amino acids, 1% sodium pyruvate, and 2% penicillin-streptomycin mix. For infections, pMEFs were plated in 12-well plates at 2.10^5 cells per well and cultured with rNiV-eGFP at a multiplicity of infection (MOI) of 0.3 plaque-forming units (PFUs)/cell for 1 h at 37°C. Virus-containing medium was then removed, and cells were washed once with 1× phosphate-buffered saline. Finally, fresh DMEM was added to cells that were incubated for 24 h at 37°C. Human male monocytic THP-1 cell lines WT, cGAS KO or STING KO were obtained (Mankan et al., 2014) and cultured in RPMI 1640 GlutaMAX supplemented with 10% heat-inactivated FBS, 1% HEPES and 2% of penicillin-streptomycin mix. Human pulmonary microvascular endothelial cells (HPMEC) (Krump-Konvalinkova et al., 2001) were from a male donor and cultured in Endothelial Cell Growth Medium, in flasks coated with 0,1% bovine gelatine in PBS. For infection, HPMECs were plated in 12-well plates at 2.10^5 cells per well and cultured with rNiV-eGFP or rMeV-edmH-eGFP at a MOI of 1 PFUs/cell for 24 or 48 hours at 37°C. All cell types were incubated at 37°C with 5% CO2 and were tested negative for Mycoplasma spp.

Ethical statement

Animals were handled in strict accordance with good animal practice as defined by the French national charter on the ethics of animal experimentation and all efforts were made to minimize suffering. Animal work was approved by the Regional ethical committee and French Ministry of High Education and Research and experiments were performed in the INSERM Jean Mérieux BSL-4 laboratory in Lyon, France (French Animal regulation committee N° 00962.01).

METHOD DETAILS

Infection of mice

Groups (male and female) of 5–10 mice from each line, 4–6 weeks of age, were anesthetized with isoflurane and infected intraperitoneally with 10^6 PFUs of Nipah virus Malaysia strain, contained in a 200 µL volume. Animals were monitored for 24 days after infection and manipulated in accordance to good experimental practice and approved by the regional ethics committee CECCAPP (Comité d'Evaluation Commun au Centre Léon Bérard, à l'Animalerie de transit de l'ENS, au PBES et au laboratoire P4) and authorized by the French Ministry of Higher Education and Research (no. 00962.01). Animal experiments were conducted by the animal facility team in the INSERM Jean Mérieux BSL-4 laboratory in Lyon, France.

Drugs

H151, a specific inhibitor for STING and RU.521, a specific inhibitor for cGAS were added 1 h previous infection of THP-1 cells at 10 µM and 10 µg/ml, respectively, selected according to the previously published results (Chang et al., 2020; Hayden et al., 2020). Then, cells were infected with rNiV-eGFP or rMeV-edmH-eGFP and incubated for 24 or 48 h at 37°C with 5% CO2.

Viruses

NiV Malaysia (isolate UMMC1; GeneBak AY029767, recombinant NiV (rNiv)–enhanced green fluorescent protein (eGFP) (Yoneda et al., 2006) and recombinant MV IC323 vaccine strain, expressing Edmonston H and eGFP (Hashimoto et al., 2002), kindly provided by Dr Y. Yanagi (Kyushu University, Japan) and were prepared by infecting Vero-E6 cells, in the INSERM Jean Mérieux biosafety level 4 (BSL-4) and BSL-2 laboratories at CIRI in Lyon, France respectively.

Immunohistochemistry

Brains from mice were embedded in paraffin wax and sectioned at 7 μm. Slides were deparaffinated and rehydrated in three Xylene baths for 5 min each, followed by two 100% alcohol baths for 5 min, and then succeeded with multiple baths using decreasing level of alcohol for 3 min each. After deparaffination, slides were put in a sodium citrate solution in a boiling water bath for 20 min for heat-induced epitope retrieval and washed 3 times in PBS for 3 min afterwards. Activity of endogenous peroxydase was blocked using a H2O2 0.3% solution. Blocking of non-specific epitopes is done using PBS-2.5% decomplemented Normal Horse Serum + 0.15% Triton X-100 for 30 min. Then, primary rabbit anti-NiV N antibody was used at 1/10000 dilution and incubated overnight at 4°C in the blocking buffer. For secondary antibody and revealing steps, ImmPress system (anti-rabbit ig/peroxydase) was used. Counterstaining was performed using Harris solution and photographs were taken with a microscope Zeiss Axiovert 100M.

Co-immunoprecipitations

HPMEC cells (5×10^5) were seeded in 6-well plates. 16 h after seeding, cells were infected with the appropriate dilution of rNiV-eGFP or rMeV-edmH-eGFP at a MOI of 1 in RPMI described above. Forty-eight hours post-infection, cells were lysed in RIPA buffer, supplemented with a cocktail of protease-phosphatase inhibitors for 30 min on ice, and centrifuged for 10 min at 4°C at 15,000 g. Supernatants were incubated with a rabbit anti-STING antibody for 2 h at 4°C. Then, protein A/G agarose beads were added to the mix overnight at 4°C. Beads were then washed three times in washing buffer (RIPA buffer, supplemented with a cocktail of protease-phosphatase inhibitor), and proteins were eluted in 100 μl of elution buffer (Reducing agent 10X, Laemmli 4X, RIPA buffer, supplemented with a cocktail of protease-phosphatase inhibitors) for 15 min at 96°C. Then the eluate and a sample of input of the cell extract were run on polyacrylamide gel electrophoresis (SDS-PAGE) and analyzed by western-blotting.

Immunoblot analysis

Heated protein lysates were separated by 4-15% SDS-PAGE and electro transferred for 1 h onto polyvinylidene difluoride (PVDF) membranes at 4°C. PVDF membranes were blocked in Tris-buffered saline containing 0.05% Tween 20 (TBS-T) + 5% milk for 1 h and then incubated overnight with primary antibodies, mouse anti-GAPDH, rabbit anti-STING, rabbit anti-human S366 p-STING, rabbit anti-mouse S365 p-STING, rabbit anti-Caspase 3, rabbit anti-cleaved Caspase 3 and rabbit anti-Ub-K63 antibodies, diluted 1:1000 in TBS-T + 0.2% milk. Membranes were then washed 3 times using TBS-T and incubated on an additional 1 h with horseradish peroxydase conjugated anti-mouse or anti-rabbit IgG antibodies (diluted 1:5000 in TBS-T + 5% milk). Membranes were then washed 5 times in TBS-T, incubated in Super Signal West Dura to stain cell lysates or in Super Signal West Femto reagent to stain bead eluates. Chemiluminescent signals were measured with the VersaDoc and ChemiDoc Imaging System.

RNA extraction and RT-qPCR

At indicated time points, cells and supernatants were collected and RNA extracted using appropriate NucleoSpin RNA Kits according to the manufacturer's instructions. Equal amounts of extracted RNA (500 ng) were reverse transcribed using the iScript Select cDNA Synthesis Kit and amplified by real-time PCR using Platinum SYBR Green qPCR SuperMix-UDG on a StepOnePlus Real-Time PCR System. Pfaffl Model (Pfaffl, 2001) and Bustin MIQE checklist (Bustin et al., 2009) were used for all validations and calculations. To validate the efficacy of our primers, a PCR on a positive control (cDNA from corresponding stimulated cells) has been performed before dosing several dilutions of our PCR products using the Denovix DS-11-FX spectrophotometer to evaluate the quantity of DNA in each dilution. Then, the PCR products were 10-fold serially diluted with a range from 10^{-3} to 10^{-12} to validate efficacy, specificity and sensitivity of each couple of primers used for qPCR. Moreover, the exact number of copies in each qPCR reaction was obtained by calculating the "N0 Samples = N0 Standard * Efficacy$^{-\Delta Ct}$" before being converted using molecular weight of each targeted gene and Avogadro number. Results obtained were either kept as "copies/ml" for supernatants or converted to "copies/μg of RNA" for cell lysates. Finally, normalization was performed by dividing obtained numbers of RNA copies of the target genes with the deviation of the glyceraldehyde 3-phosphate dehydrogenase (GAPDH) used as house-keeping gene. Specific set of primers were designed and validated for the detection of human hGAPDH, hIFNα and hIFNβ, murine mGAPDH, murine mIFNα and mIFNβ and viral NiV N and MeV N.

Immunofluorescence

For PMEFs and THP-1 infections, 3×10^5 and 5×10^5 cells were seeded in 12-well plates, respectively, before being infected with rNiV-eGFP and rMeV-edmH-eGFP at a MOI of 0.3 or 0.1 and cultured for 24 or 48 h at 37°C with 5% CO2. Then, cells were evaluated for eGFP expression using a Zeiss Axiovert 100M microscope in the BSL-4 or a NIKON Eclipse Ts2R in the BSL-2, and photographs were taken 24 and 48 h after infection and treated using ImageJ software version Java 1.8.0_112.

Flow cytometry

THP-1 cells were seeded in 12-well plates at 3×10^5 and 5×10^5 per well before being infected with rNiV-eGFP and rMeV-edmH-eGFP at a MOI of 0.1 and cultured for 24 or 48 h at 37°C with 5% CO2. Then, cells were washed, reconstituted in PBS 1X and evaluated for eGFP expression using a Gallios flow cytometer in the BSL-4 or a 4L Fortessa flow cytometer. Analyses were performed 24 and 48 h after infection.

QUANTIFICATION AND STATISTICAL ANALYSIS

Analysis of eGFP quantification in THP-1 cells

The results are presented in the form of histograms which represent the mean eGFP positive cells for each conditions and error bars represent the standard errors (SE) for n=3 experimental replicates. The different conditions were compared to the control (WT+). Statistical significance was assessed by a one-way ANOVA, followed by a Tukey's multiple comparisons test; *$p < 0.05$, **$p < 0.01$, ***$p < 0.001$ and ****$p < 0.0001$ (threshold of significance of 5%).

qPCR analysis

The results are presented in the form of histograms, which represent the mean of copies of mRNA for a gene for each condition and error bars represent the standard errors (SE) for n=3 experimental replicates. The different conditions were compared to the control (WT+). Statistical significance was assessed by a one-way ANOVA, followed by a Tukey's multiple comparisons test; *$p < 0.05$, **$p < 0.01$, ***$p < 0.001$ and ****$p < 0.0001$ (threshold of significance of 5%).

Densitometry

Densitometric analyses of cleaved caspase 3 immunoblots from three independent experiments were performed using the VersaDoc Imaging System (Bio-Rad) and analyzed with ImageJ 1.52p Fiji package software (https://imagej.net/Fiji). GAPDH expression was used for normalization. The results are presented in the form of histograms and error bars represent the standard errors (SE) for n=3 independent experiments.